Earth Energy Science 1 (2025) 228–241

Contents lists available at ScienceDirect

Earth Energy Science

journal homepage: www.keaipublishing.com/en/journals/earth-energy-science/

Impact of salinity on spontaneous emulsification near water/oil interfaces

Lifei Yan[a,b,*], Amir Raoof[b,**], Senyou An[c,**]

[a] Faculty of Civil Engineering and Geosciences, Delft University of Technology, Stevinweg 1, Delft, CN 2628, the Netherlands
[b] Department of Earth Sciences, Utrecht University, Princetonlaan 8a, Utrecht 3584 CB, the Netherlands
[c] State Key Laboratory of Intelligent Construction and Healthy Operation and Maintenance of Deep Underground Engineering, College of Civil and Transportation Engineering, Shenzhen University, Shenzhen 518060, China

ARTICLE INFO

Keywords:
Spontaneous emulsification
Nano- and micro-scale emulsion
Dynamic light scattering
Pendant drop experiment
Salinity effect

ABSTRACT

Natural surfactants that are present in complex crude oil may induce spontaneous emulsification in the oil and brine phases that co-exist in rock pores. This process is known to be affected by the salinity of brine. However, the role of salinity in water-oil micro-emulsification is not fully understood. In this paper, we report on our experimental studies of the effect of salinity on spontaneous emulsification in a "mixture" of dodecane and brine. The dodecane contains SPAN 80 surfactant and brine with different salinity values, varying from 0.2 % to 20 % (by weight). For our observations, we use dynamic light scattering (DLS) technique to capture nano-scale emulsion formation and pendant drop method to observe micro-scale emulsion dynamics. The DLS experiments show that small (2.2 nm) and medium-sized emulsions (100 nm) are formed at low salinities, while at higher salinities only smaller droplets are formed and emulsification is reduced. In pendant drop experiments, dodecane and heptane systems were tested over 13 h. Heptane exhibited faster emulsification at water-oil interfaces in the cases with pure water and low salinity brine (0.2 %), where the changes at interfacial area occurring within two hours and significant droplet shrinkage by 13 h. Lower salinity enhances micelle activity and emulsification, while higher salinities (2 %, 5 %, and 20 %) stabilize the oil-water interface and suppress emulsion formation. Dodecane exhibits a similar trend in emulsification but forms more stable emulsions and maintains a more stable water-oil interface compared to heptane. Additionally, we present the theory of reverse micelle exclusion through a theoretical derivation, providing a deeper understanding of the emulsification mechanism. Four distinct scenarios are schematically presented to explain the influence of salinity on spontaneous emulsification, illustrating how varying salinity levels affect micelle formation and emulsion behaviour. This study provides valuable insights into optimizing salinity levels in enhanced oil recovery.

1. Introduction

The process of micro-dispersion and emulsification has been extensively researched to gain a deeper understanding of the interactions between saline water and crude oil (Yan et al., 2020). Emulsions are typically classified into water-in-oil (W/O), oil-in-water (O/W), and more complex multiple emulsions (W/O/W or O/W/O). Although all types may occur during water flooding, W/O and O/W are the most commonly observed (Martínez-Palou et al., 2013). Surfactants, which commonly have hydrophilic and hydrophobic ends, position themselves at the oil-water interface, lowering surface tension and facilitate spontaneous emulsion formation from the nano- to pore-scale (Rodríguez-Hakim et al., 2020). Studies by Rosen and Kunjappu (2012) and Israelachvili (2011) provide foundational insights into surfactant adsorption kinetics and micelle formation, which govern interfacial tension reduction critical for emulsification. Spontaneous emulsification occurs when two immiscible liquids interact without the input of external energy, reaching a thermodynamically stable state at a minimal free energy state (López-Montilla et al., 2002). When surfactants exist within water or oil, and they reach their critical micelle concentration (CMC), they organize themselves near the oil-water interface, forming micelles that encapsulate molecules that are otherwise insoluble in water or oil. For example, surfactants that are extant in water, form micelles that encapsulate oil molecules. This phenomenon increases the solubility of oil in water. The reverse may happen too, i.e., polar compounds naturally present in crude oil, such as naphthenic

* Corresponding author at: Faculty of Civil Engineering and Geosciences, Delft University of Technology, Stevinweg 1, Delft, CN 2628, the Netherlands.
** Corresponding authors.
E-mail addresses: l.yan@tudelft.nl (L. Yan), a.raoof@uu.nl (A. Raoof), senyouan@szu.edu.cn (S. An).

https://doi.org/10.1016/j.ees.2025.07.003
Received 5 May 2025; Received in revised form 17 June 2025; Accepted 17 July 2025
Available online 1 August 2025

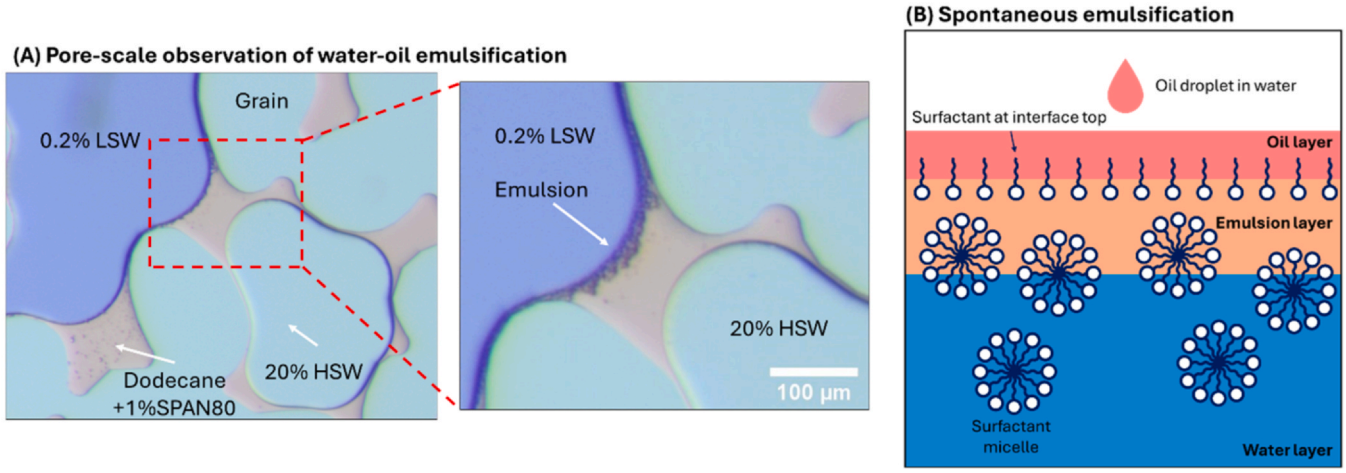

Fig. 1. (A) Microfluidic observation of spontaneous emulsification at the interface of 0.2 % LSW (low-salinity water, dark blue), 20 % HSW (high-salinity water), and Dodecane with 1 % SPAN80 surfactant after 24 h, showing emulsion formation along grain boundaries (get permission from Yan et al., 2023). (B) Schematic of the spontaneous emulsification mechanism at the oil-water interface, highlighting the diffusion of oil into the surfactant-rich water phase, formation of micelles, and the enhancement of emulsification by Marangoni roll cells.

acids, resins, and asphaltenes, can act as surfactants, form micelles that encapsulate water molecules. There are commonly referred to as reverse micelles. Both of these phenomena lead to emulsion formation (Li et al., 2020). A standard reverse micelle, spherical in shape with a diameter of around 50 Å, typically contains about 100 surfactant molecules (Goyal and Aswal, 2001). Numerous laboratory experiments have confirmed that emulsions form when crude oil interacts with water during water flooding.

The following figures provide a visual representation of these processes, demonstrating how salinity gradients and surfactant presence influence emulsion formation at the microscale. Fig. 1 (A) illustrates spontaneous emulsification in a microfluidic environment, showing interactions between oil, surfactant, and water phases with differing salinities. In the left image, the fluid system contains 0.2 % LSW (low-salinity water shown in dark blue), 20 % HSW (high-salinity water, light blue or turquoise), and dodecane with 1 % SPAN80 surfactant (shown in pink), creating clear boundaries between phases. The zoomed-in section on the right highlights the formation of an emulsion, visible as a dark band with a white arrow at the LSW-oil interface, where the salinity gradient plays a crucial role in promoting emulsification (Yan et al., 2023). The surfactant, SPAN80, lowers the interfacial tension between dodecane and water, encapsulating oil droplets to form stable oil-in-water emulsions. The salinity contrast between the low and high-salinity water affects surfactant behaviour and oil droplet stabilization (Kokal, 2005), meaning that LSW provides favourable conditions for spontaneous emulsification while HSW's high ionic strength contributes to emulsion stability (Yan et al., 2022). The salinity difference also drives Marangoni flows at the interface, enhancing surfactant transport within the water-oil interface and emulsion droplet dispersion. Marangoni flows occur when surface tension varies along an interface, causing fluid to move from low to high surface tension areas. In surfactant systems, this flow transports surfactant molecules, promoting mixing and breaking up emulsion droplets. This dynamic helps control droplet size and stability, playing a key role in emulsification (Stone, 1994). Together, these interfacial dynamics and salinity gradients result in the continuous formation of a stable emulsion, demonstrating the complex interplay of diffusion, surface tension, and fluid flow.

Fig. 1 (B) elucidates the phenomenon of spontaneous emulsification at an oil-water interface. At the interface, the oil layer (pink) overlays the water phase (blue), where surfactant molecules align with their hydrophilic heads facing the water and hydrophobic tails toward the oil, thereby reducing interfacial tension and facilitating emulsion layer formation. This alignment allows oil molecules to penetrate into the water phase, where they encounter surfactant micelles structures composed of surfactants with hydrophobic cores that encapsulate oil molecules to form swollen micelles. Such behaviour typifies a Winsor Type I emulsion, where oil-in-water (O/W) emulsions are stabilized by surfactants dispersed in the aqueous phase, resulting in nanoscale droplets without the need for external energy input. The spontaneous emulsification is driven by chemical potential differences between phases and facilitated by the surfactants. An essential enhancement of this process is the Marangoni effect, which induces convective flows due to surface tension gradients, redistributing surfactants and oil droplets to ensure efficient dispersion and stabilization of the emulsion (Zheng et al., 2022). The flow helps replenish surfactants at the interface, preventing saturation and sustaining the emulsification. Overall, the schematic captures the dynamics of emulsification—a process governed by diffusion, surfactant micellization, and interfacial flows.

Having outlined the fundamental interfacial dynamics, it is important to examine how varying electrolyte concentrations affect emulsion characteristics and stability. Several studies have investigated the link between electrolyte concentration and emulsion size. Maaref and Ayatollahi (2018) created water-in-oil emulsions using various synthetic seawater samples designed to mimic the composition of waters from the Persian Gulf, Mediterranean, Red Sea, and North Sea. Their analysis, which applied a log-normal function to describe emulsion droplet size distribution, revealed that emulsions formed under low-salinity conditions were more stable and uniform. In another study, Behera et al. (2014) explored the impact of surfactant, salt, and oil concentrations on foam formation in micellar solutions. Their results showed that as surfactant concentration increased, the foam volume generated in a blender test also increased, whereas higher salt concentrations reduced the foam volume. Additionally, increasing surfactant concentration and decreasing salt concentration were found to reduce surface tension. Du et al. (2019) observed the dynamic formation of water-in-oil (W/O) emulsions, which contributed to improved oil displacement efficiency. In a different study, Salehpour et al. (2021) conducted both static and dynamic micro-scale experiments to explore how fluid-fluid interactions affect flow behaviour and oil recovery during low-salinity waterflooding (LSWF). They documented an intensified spontaneous generation of W/O emulsions at the interface, particularly at lower flow rates, along with pressure fluctuations caused by the splitting and rupture of emulsions. Bahtz et al. (2016) emphasized the significance of controlled water mass transport in maintaining emulsion stability and thickening. They described a two-phase water transport process during spontaneous emulsification: an initial phase

driven by structural changes in the oil layer that allowed rapid, osmotically driven water transport, followed by a second phase dominated by osmotic forces. These structural changes in the oil phase were aided by the spontaneous formation of tiny water droplets, which was triggered by the presence of an oil-soluble surfactant. Zabar et al. (2020) observed a similar effect, where increasing NaCl concentrations from 0 to 5 M led to the formation of smaller oil-in-water emulsions. Furthermore, increasing the oil chain length from C7 (n-heptane) to C16 (n-hexadecane) resulted in a 58.6 % reduction in emulsion droplet size.

Despite extensive experimental studies, the detailed dynamics of emulsification—especially its influence on water transport through oil layers under varying salinity—remain not fully understood, highlighting the need for further quantitative analysis. However, a detailed understanding of the dynamics of emulsification and its precise effect on water transport through oil layers remains incomplete. While volume expansion of saline water might resemble osmosis when viewed on a macroscale, it is still unclear whether the organic phase can be treated as a rigid membrane, and there is insufficient evidence to support this assumption. Additionally, the behaviour of water transport through the oil phase, driven by salinity contrasts, is not yet fully understood. Therefore, further quantitative analysis of salinity's impact is required to clarify these processes, along with more comprehensive descriptions of dynamic emulsification and its role in water transport through an oil layer.

This paper is structured as follows: Section 2 discusses water transport caused by reverse micelle formation in the oil phase and its implications for emulsification. Section 3 describes the experimental setup for measuring interfacial behaviour, including Dynamic Light Scattering (DLS) and pendant drop tensiometer, to understand factors that affect emulsion size and interfacial tension. Section 4 analyses the effects of salinity on spontaneous emulsification at the water-oil interface, presenting key results from experiments on how salinity influences emulsion formation and size distribution over time. Section 5 provides direct observations of emulsion generation processes, highlighting how different salinity levels alter emulsion dynamics and stability at the interface. Finally, Section 6 concludes with insights on water transport mechanisms, implications for oil recovery, and the overall influence of salinity on emulsion behaviour, offering a comprehensive summary of our findings and suggesting potential avenues for future research.

2. Theory of water transport through oil by inverse micelle

Regarding the case of water transport in the oil phase, it is essential to examine the water flux driven by the movement of emulsion droplets. During the formation of reverse micelles at the interface, certain salt ions become encapsulated by a water shell inside the micelles as salt hydrates (Pays et al., 2002). The amount of ions trapped within the micelles is much smaller compared to the water shell surrounding them, as the dominant component of reverse micelles is water (Cheng et al., 2007).

In an earlier study, Wen and Papadopoulos (2000) employed capillary video-microscopy to observe water transport between two aqueous phases across an intervening oil layer under osmotic pressure. Fig. 2 illustrates the water is transport from the droplet of water + surfactant into the oil phase though the expulsed reverse micelles. In the initial stage t = 0, the water droplet, containing surfactant molecules, is in contact with the surrounding oil phase. At this point, the surfactant remains predominantly within the water droplet. The spontaneous emulsification begins with reaching CMC and the surfactant molecules migrate to the water-oil interface between the water and oil, as depicted in the middle panel, with their hydrophilic heads facing the water and hydrophobic tails extending into the oil. This alignment reduces the interfacial tension, facilitating the formation of water-in-oil (W/O) emulsions, where water droplets are dispersed within the continuous oil phase. This process occurs spontaneously, without external energy, as the system reaches a thermodynamically stable state. In the final stage, shown in the right panel, reverse micelles form and are expelled into the oil phase. These micelles, with water molecules encapsulated within their hydrophilic cores, are stabilized by surfactants and further dispersed throughout the oil. Their experiments revealed that tiny emulsion droplets spontaneously formed at the water-oil interface, detaching and moving into the oil phase within 30 min of contact between the water and the surfactant-laden oil. However, when using high salinity aqueous drops (≥5 M NaCl), no spontaneous emulsification was observed in the SPAN-containing n-hexadecane.

We now examine the diffusion of micelles driven by electrostatic interactions and formulate a transport law for micelle movement. This transport law has the same form as Fick's law but involves a diffusion coefficient, D_m, which is proportional to the micelle concentration, C_m. As shown in Fig. 3, when two micelles come close enough to penetrate each other's electric double layers, they experience electrostatic repulsion. This layer of charges, referred to as the diffuse electric double layer, has a characteristic thickness known as the Debye length, r_0, which typically ranges from 1 to 5 nm. Once these electrostatic forces are activated, the micelles begin to move in response to their hydrodynamic mobility.

Two reverse micelles, separated by a distance r, exert an electric force on each other.

$$\mathbf{f} = \frac{q^2 \boldsymbol{u}_r}{4\pi\varepsilon_0 r^2} e^{-\frac{r-2a}{r_0}} \tag{1}$$

where q denotes the charge on the micelle, ε_0 is the vacuum permittivity, a represents the micelle radius, r_0 refers to the Debye length (typically ranging from 1 to 5 nm), and $\boldsymbol{u_r}$ is the unit vector along the r-axis. The thickness of the diffuse electric double layer in the liquid is given as $r - 2a$. The exponential function serves as a cut-off to the interaction range between micelles. The total force acting on a micelle is determined by contributions from all its neighbouring micelles, which can be represented by the concentration field $C_m(\boldsymbol{r})$, describing the number of particles per unit volume. Using a mean-field approximation, the total force can be expressed by:

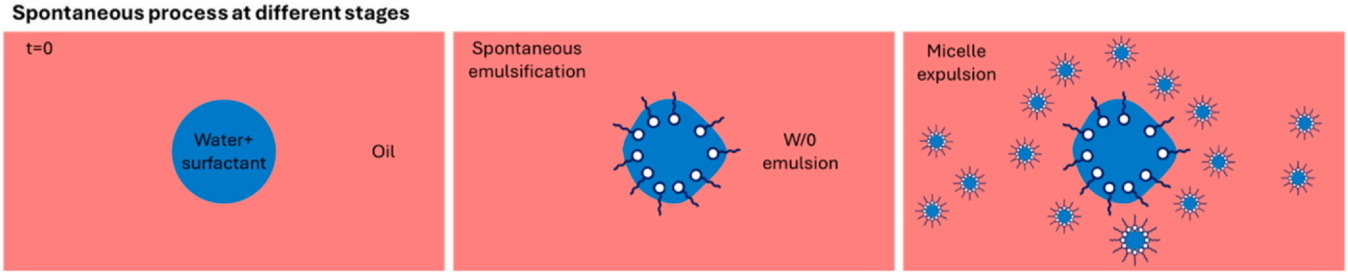

Fig. 2. Schematic of spontaneous emulsification process in W/O system (adapted from Wen and Papadopoulos 2000). The process begins with a water droplet containing surfactants in contact with oil (t = 0). Surfactants align at the interface, leading to the formation of a water-in-oil (W/O) emulsion. In the final stage, reverse micelles form and are expelled into the oil phase, stabilizing the emulsion system.

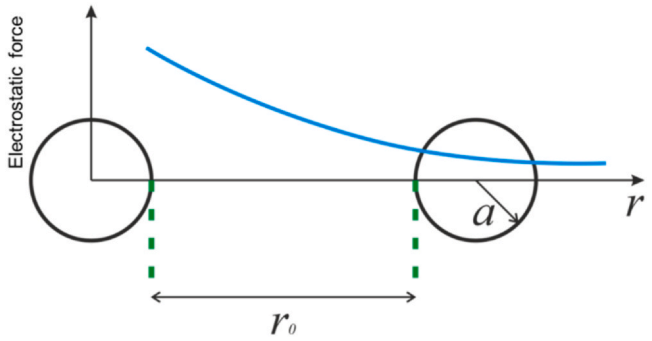

Fig. 3. Illustration of mobile charge distribution surrounding two micelles. $\boldsymbol{a}$ is the radius of one micelle.

$$\mathbf{F} = \int dVC_m(\boldsymbol{r})\mathbf{f} \tag{2}$$

If the concentration $Cm(\boldsymbol{r})$ remains constant, this force integrates to zero due to symmetry given by,

$$C_m(\boldsymbol{r}) = C_0 + \mathbf{r}\cdot\nabla C_m \tag{3}$$

where C_0 is the value of concentration field at $r = 2a$. In spherical coordinates, and aligning the z-axis with the gradient of the concentration field, ∇C_m, we express the force as

$$\mathbf{F} = \int dV\boldsymbol{r}\cdot\nabla C_m\mathbf{f} \tag{4}$$

which has a non-zero component only along the z-direction. Since $(\boldsymbol{u}_r)_z = \cos\theta$, the total force is derived as

$$\mathbf{F} = \int dV\boldsymbol{r}\cdot\nabla C_m\cos\theta f(r) = 2\pi\int_0^{\pi} d\theta\sin\theta\cos^2\theta\int_{2a}^{\infty} drr^3 f(r)|C_m| = \frac{q^2r_0^2}{3\varepsilon_0}\nabla C_m \tag{5}$$

This force is balanced by the hydrodynamic drag, resulting in the micelle flux J_m (number of micelles crossing per unit area per time) as outlined in

$$\boldsymbol{J_m} = C_m\mu_m\mathbf{F} \tag{6}$$

where μ_m represents the mobility of a micelle. Substituting the expression for the force, **F** into this equation yields the flux in the form of Fick's law, as shown as

$$\boldsymbol{J_m} = D_m\nabla C_m \tag{7}$$

with the corresponding diffusivity given by:

$$D_m = \mu_m\frac{q^2r_0^2}{3\varepsilon_0}C_m \tag{8}$$

Now, the mobility may be approximated by the Stokes formula

$$\mu_m = \frac{1}{6\pi\eta a} \tag{9}$$

where η represents the viscosity of the surrounding oil.

Comparing the magnitude of the micelle diffusivity D_m with the molecular diffusion constant $D_w = k_BT\mu_w$ for water in oil, the ratio of the two diffusion constants is given as

$$\frac{D_w}{D_m} = (C_mr_0^3)\frac{\delta}{a}\frac{q^2}{k_BT3\varepsilon_0r_0} \tag{10}$$

Here, $N_D = Cr_0^3$ refers to the number of neighboring micelles within the Debye length, δ/a is the ratio of molecular size to micelle size, and the final term represents the ratio of the micelle's electrostatic energy to its thermal energy. Using typical values such as $q = ze$, $r_0 = 3$ nm and room temperature T, the ratio is expressed as

$$\frac{q^2}{k_BT3\varepsilon_0r_0} \approx 100z^2 \tag{11}$$

To ensure that $D_w \gg D_m$, the charge number must satisfy the relationship

$$z \gg \sqrt{\frac{a}{100\delta}N_D} \tag{12}$$

which holds for moderate values of z and $N_D \sim 1$. Thus, the electrostatic forces driving micelles can lead to water transport that may surpass molecular diffusion.

The flux of water, $\boldsymbol{J_w^{micelle}}$, in terms of the number of micelles per unit area per unit time, can be expressed as

$$\boldsymbol{J_w^{micelle}} = \boldsymbol{J_m} = -\frac{q^2r_0^2}{18\pi\eta\varepsilon_0a}\frac{C_m}{N_A}\nabla C_m \tag{13}$$

where N_A represents the Avogadro constant.

3. Experimental approach and material property

3.1. Dynamic light scattering set-up

The measurement of micelle size within emulsions is performed using Dynamic Light Scattering (DLS), a method widely employed for determining the size distribution of small particles in suspensions or polymer solutions. The DLS system used in this study, the Zetasizer Nano ZS90 from Malvern Panalytical, is particularly effective for detecting particles in the range of 0.3 nm to 10 μm, as shown in Fig. 4 (A) and (B). The device is sensitive to even low concentrations of larger particles or aggregates, as the intensity of scattered light scales with the sixth power of particle size. In DLS, a monochromatic laser beam is passed through a polarizer and directed into the sample chamber. The scattered light, influenced by particle Brownian motion, passes through a second polarizer and is collected by a detector (photomultiplier). The Brownian motion of particles induces fluctuations in the scattered light intensity. These fluctuations are analyzed to determine the velocity of the particles, which is then used to calculate their size using the Stokes-Einstein equation. The DLS setup offers flexibility for measurements in both dilute and concentrated suspensions. For dilute samples, the system maximizes the measurement volume to minimize laser flare, while for concentrated samples, the path length is minimized to reduce multiple scattering events. When preparing the sample for the Zetasizer, the fluid needs to be placed in a cuvette. For our experiments, clean cuvettes made from optically clear disposable plastic, similar to the one shown in Fig. 4 (B), with dimensions of 3 × 3 mm, 5 × 5 mm, or 10 × 10 mm, are used. It is crucial to keep the sample inside the cuvette clean and free from any visible particle sedimentation. The minimum volume required for accurate measurement varies depending on the model. The Zetasizer we used requires at least 12 μL. However, preparing 1 mL of sample is recommended to ensure that the height of the sample is higher than the laser height. To investigate properties of emulsions formed through spontaneous emulsification, the experimental setup involved placing a layer of brine at the bottom of the cuvette, followed by a gently placing a layer of oil on top of it. The height of the emulsion formation zone (~6.5 mm) is positioned slightly below the laser detection height (8 mm) to accurately capture changes in emulsion size over time.

The Non-Invasive Backscatter (NIBS) technology, illustrated in Fig. 4 (C), detects scattered light at a 173° angle, optimizing sensitivity and allowing for accurate size measurements across a broad concentration range. The relevant particle concentration across a range from 0.1 to 40000 ppm, enabling measurement of the widest range without any need for dilution. DLS provides detailed measurements that include various peak statistics of particle intensity such as mean size, mode, width, and the area under the size distribution curve. The acquired DLS size distribution represents the heterogeneous nature of the micelles in the emulsion. The combined use of DLS technology and advanced detection methods such as NIBS enables accurate and precise measurements of micelle sizes within a wide concentration range,

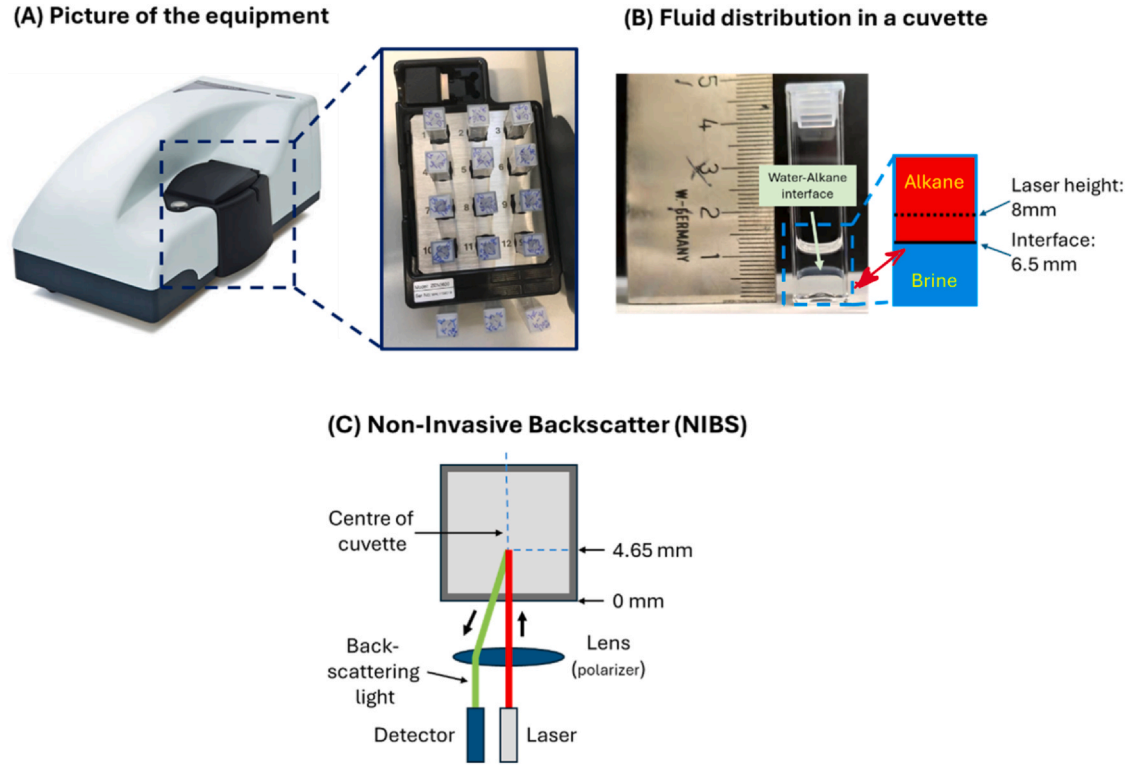

Fig. 4. Images of the DLS setup. (A), the analyser instrument with a zoomed-in view of the tray containing multiple sample cells. (B), the distribution of liquid in one cuvette for the Zetasizer equipment. (C), schematic of a DLS system, including a laser, detector, focusing lens and cuvette for a NIBS configuration.

allowing for the detailed characterization of the emulsion's micelle population.

3.2. Pendant drop experimental set-up

In our experimental setup, the equipment, KRÜSS DSA100E, is used to measure interfacial tension of water (or brine with high salinity) droplet in alkane for studying the impact of salt in water on spontaneous emulsification through pendant drop tensiometer. The schematic of the setup is shown in Fig. 5. It is designed for precise measurements of interfacial tension, offering images up to 2300 frames per second, and is controlled by sophisticated software that provides data acquisition and analysis. The system's high-precision syringe dosing for generating water droplet and temperature-controlled cuvettes containing oil phase enabled us to maintain consistency across trials. The water droplet with a size of around 9 μL can be formed by the syringe. After reaching the desired size, the droplet is hanged at the bottom of the syringe needle and suspends in an alkane environment containing 1 % SPAN 80 emulsifier.

The brine droplet's size and interfacial tension are continuously recorded using a CCD camera over a period of five hours. The shape

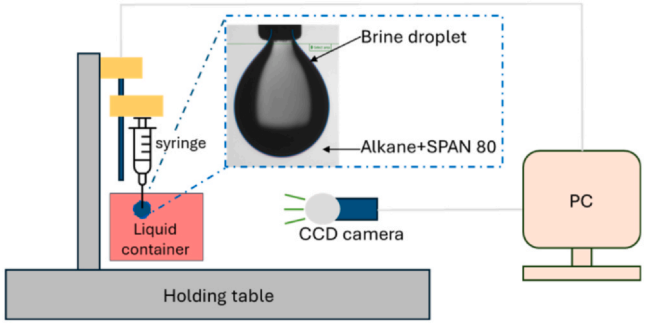

Fig. 5. Schematic of the pendant drop experimental setup.

over time is analyzed to calculate the Bond number as in Eq.14. This feature is supported by the DSA100E's built-in software, ensuring reliable results across multiple salinity levels of brine solutions (0 %, 0.2 %, 2 %, and 5 %).

$$B_o = \frac{\Delta\rho g R_0^2}{\gamma} \tag{14}$$

where the density difference is $\Delta\rho = \rho_b - \rho_d$, ρ_b and ρ_d are the brine alkane and density, respectively. R_0 is the pendant droplet diameter, γ is the interfacial tension, and g is the gravitational acceleration.

3.3. Liquid preparation and property

To investigate the emulsification process, hydrocarbon-soluble SPAN 80 (Sorbitane monooleate, HLB = 4.3) serving as an emulsifier is added to alkanes. A brine solution of 20 % w/v is synthetically created by mixing deionized water with precise amounts of salts, including NaCl, Na_2SO_4, $MgCl_2{\cdot}6H_2O$, and $CaCl_2{\cdot}2H_2O$, resulting in a 180,000 ppm solution. Other brine samples are prepared by diluting the 20 % brine to 0.2 %, 2 %, and 5 % saline solutions with salinity levels of 1800, 18,000, 45,000, and 180,000 ppm, respectively, as outlined in Table 1. An extra sample of demi-water is used for the reference experiment. We used two different oils, namely n-heptane (C_7H_{16}) and n-dodecane ($C_{12}H_{26}$), in order to study the effect of carbon chain lengths. Before starting the experiments, both alkanes are equilibrated with 1 % w/w SPAN 80 for 24 h. A concentration of 1 % w/w SPAN 80, approximately 1.75×10^{-2} mol/L, significantly exceeds the critical micelle concentration (CMC) for both alkanes (CMC of heptane is 1.8×10^{-5} mol/L and CMC of dodecane is 1.9×10^{-5} mol/L) (Peltonen et al., 2001). All chemicals, including salts and alkanes, are sourced from Sigma Aldrich.

Firstly, the brine solution is placed at the bottom of the cuvette. Then, we use the syringe to carefully place alkanes on the top of brine without disturbing the oil/brine interface. Ten samples are prepared in this fashion; these are shown in Fig. 6. The oil-water interface is initially clear and clean but becomes opaque after 24 h due to spontaneous

Table 1
The ion components of brine samples.

Ion	DIW	0.2 % Brine	2 % Brine	5 % Brine	20 % Brine
Na^+	0	499	4990	12,475	49,898
K^+	0	32	325	812	3248
Mg^{2+}	0	145	1450	3625	14,501
Cl^-	0	1118	11,181	27,953	111,812
SO_4^{2-}	0	2	23	59	234
Total dissolved solids	0	1797	17,969	44,923	179,693

emulsification, as can be seen in Fig. 6. The figure clearly shows that there is less emulsion formed with an increase in salinity. In the case of dodecane and 0.2 % salinity, a uniform dispersion of emulsions in the oil phase is observed. During the DLS experiment, the size of the emulsion droplets is measured every two hours within 24 h. In the pendant drop experiments, the droplets are continuously observed for 24 h, and the interfacial tension is determined.

4. Results and discussion

4.1. Typical dynamic change of emulsion in the dodecane and 0.2 % brine

As mentioned in the Introduction, salinity plays a critical role in emulsification processes, influencing both droplet size and the extent of emulsions. To understand the dynamic process of emulsification better, the oil/water interface in the cuvette containing dodecane + SPAN80 and 0.2 % salinity water is observed for 27 h. Images are shown in Fig. 7. At the 1-hour mark of contact between water and oil, the interface is still clean with no visible emulsion. This indicates that no significant interaction and no enough emulsion formation to be detectable near the water-oil interface. At three hours, a slight white turbidity is seen at the interface on the oil side. This reveals that the process of emulsification continuous and huge amount of emulsion are forming within the oil phase near the interface. These micelles are small, initially invisible to the naked eye, but as their concentration increases, they begin to scatter light, leading to the visible white haze. At five hours, the white layer at the interface becomes more prominent and thicker, suggesting that the concentration of emulsified droplets, driven by micelle formation and diffusion into the oil phase, has significantly increased. The formation of this layer represents the aggregation of emulsions, which are more stable due to emulsion droplets diffusion from the water into the oil. By 7 h, the white emulsion layer reaches a stable state in both colour and shape. However, the emulsion layer at 7 h is thinner than at 5 and 9 h, indicating a transient stage in the emulsification process. This temporary thinning may result from droplet coalescence or rearrangement within the emulsion, where smaller droplets merge into fewer but larger ones, causing a reduction in visible layer thickness. Such dynamic behavior suggests that emulsification involves fluctuating phases of droplet formation and destabilization before stabilizing again. The continued diffusion of water leads to the formation of a thick emulsion layer at the interface. The emulsion formation has peaked, and the system has reached a steady state in terms of micelle concentration and emulsification. The system has stabilized, and further emulsification or micelle diffusion is minimal at this point. To confirm this phenomenon, the DLS experiments is performed, and the changes of the emulsion sizes are measured.

The dynamic progresses of the size distribution of droplets during emulsification for the case of 0.2 % saltwater and alkane, as measured using DLS, is shown in Fig. 8. Initially, at 1 h, only a few emulsion droplets are detected, as shown by the peak around 70 nm, reflecting minimal interaction between the water and oil phases. As time progresses to 3 and 5 h, the size distribution changes significantly (see the details of droplet size change in Fig. 9). At 5 h, the most significant peak emerges in the mid-range size (around 100 nm), indicating that middle-sized emulsion droplets dominate the system. Small emulsion droplets (around 2.1 nm) are also present, but their population remains relatively small, around 4.2 %, showing that the middle-sized droplets are the primary contributors to the emulsion at this stage. At 14 h, small emulsion droplets continue to grow, as demonstrated by a slight rise in their proportion. The peak for larger droplets diminishes, suggesting that larger emulsion droplets may have diffused, leaving predominantly small and mid-sized droplets. After 14 h, the size of the small droplets stabilizes, maintaining a distribution around 2.2 nm. At this stage, the middle-sized droplets maintain their dominance in size distribution, but

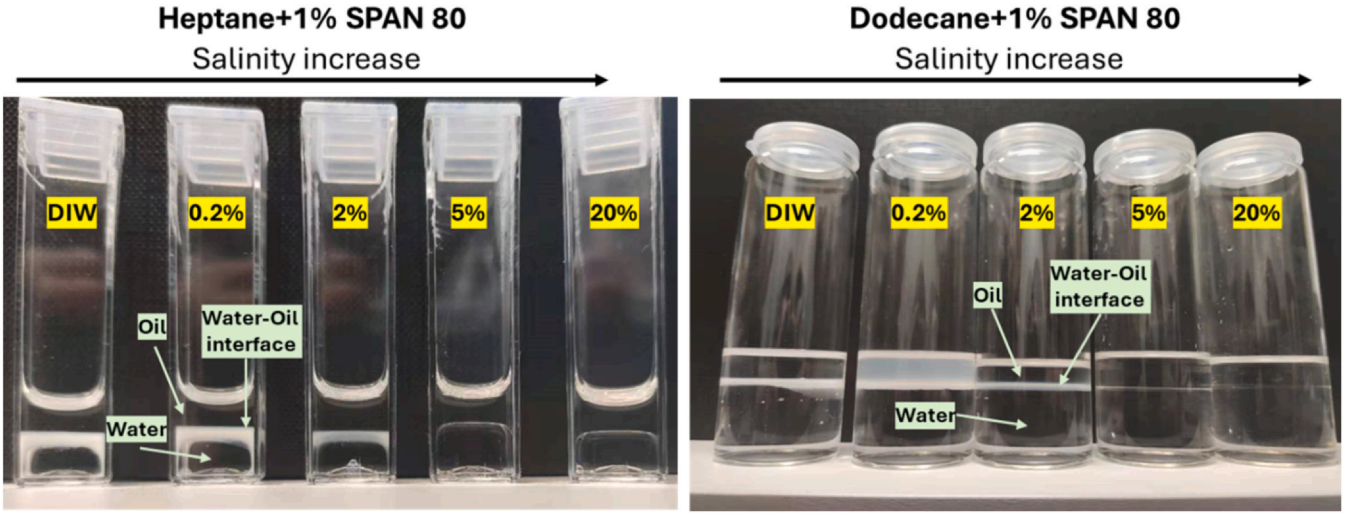

Fig. 6. Pictures of spontaneous emulsification in cuvettes after24 hours of brine/alkane contacting at room temperature. The samples with dodecane + SPAN 80 are prepared in glass bottles (ϕ 2 cm). The glass bottle is used for observing the interface, while the plastic cuvette is used for the DLS measurement throughout the experiment.

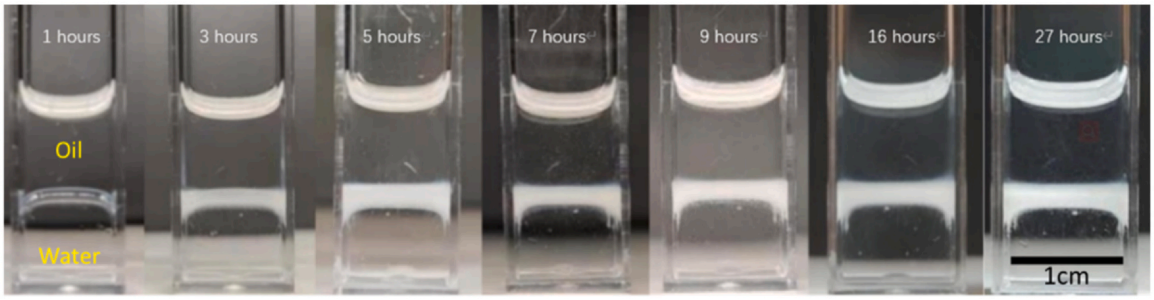

Fig. 7. Observation of spontaneous emulsification in the cuvette containing dodecane + SPAN 80 and 0.2 % salinity water for 27 h. The white regions on the top of oil layers are the light scattering between the viewing point and light.

their proportion begins to level off. As time advances to 14 and 24 h, the system reaches equilibrium. The small emulsion droplets (around 2.2 nm) and middle-sized emulsion droplets (approximately 125 nm) now share nearly equal proportions, with 52.9 % and 47.1 % of number of proportion, respectively. This trend suggests that over time, the system favours the formation of stable small and medium-sized emulsion droplets.

To gain a better understanding of dynamic changes in emulsion droplet sizes, a plot of the evolution of small, middle, and large-size micelles over a 24-hour period is provided in Fig. 9. The data provide key insights into how the distribution of emulsion droplet sizes shifts as emulsification progresses, offering a detailed view of the behaviour of emulsion droplets at different stages. At the beginning of the experiment (0–5 h), mainly medium-size droplets (10–1000 nm) are formed (black squares). However, their relative number decreases sharply after that and newly formed micelles are mainly small (1–10 nm). At around 15 h, an equilibrium is reached, and the same number of each size class are formed. The small-size droplets (red circles) start to increase in number of proportion after the first few hours. As the experiment reaches the 5–10-hour mark, the small-size droplets become more

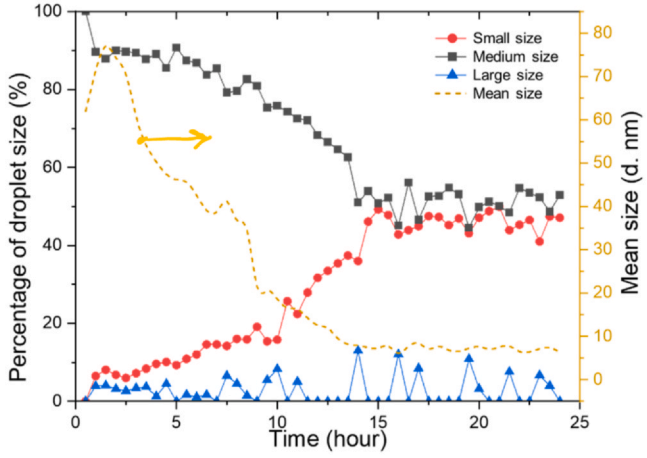

Fig. 9. Dynamic evolution of emulsion sizes over 24 h. The solid lines show the number of proportion and distribution of small, middle, and large emulsion droplets.

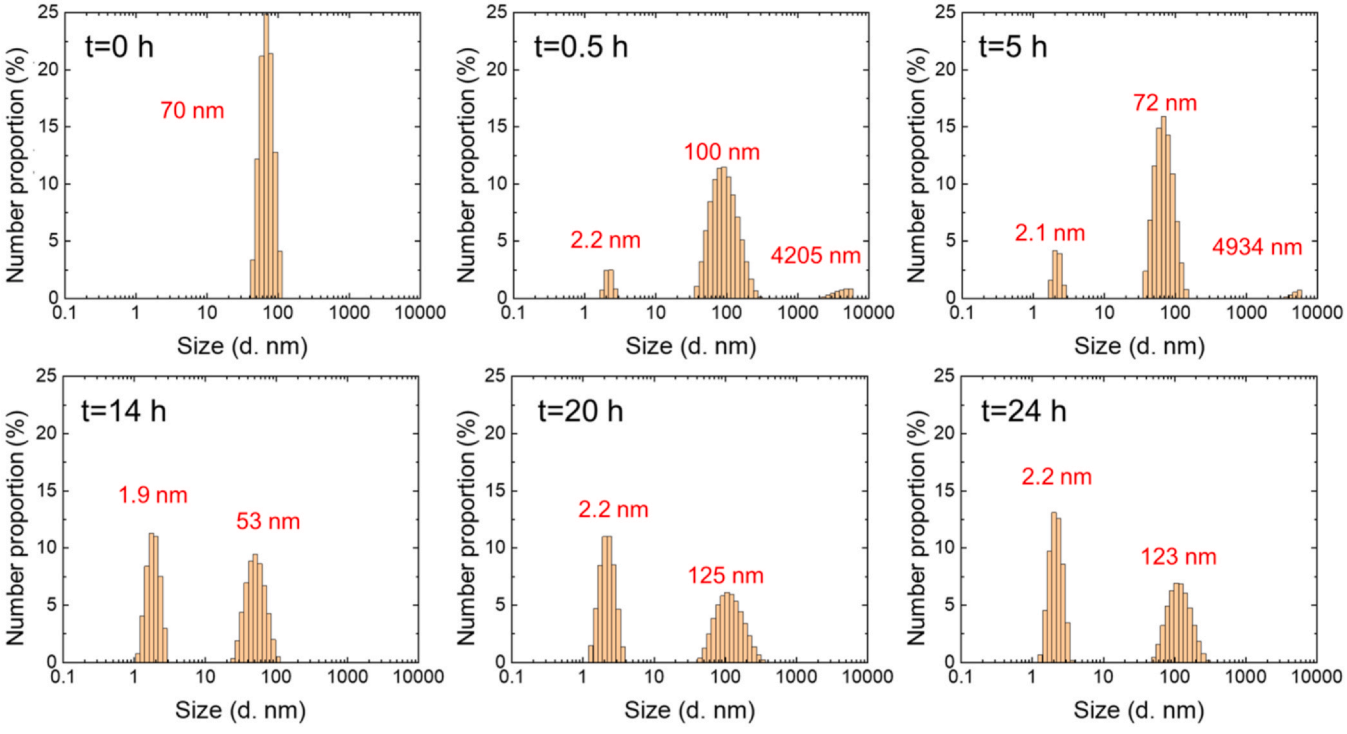

Fig. 8. Size distribution of microemulsion droplets over 24 h.

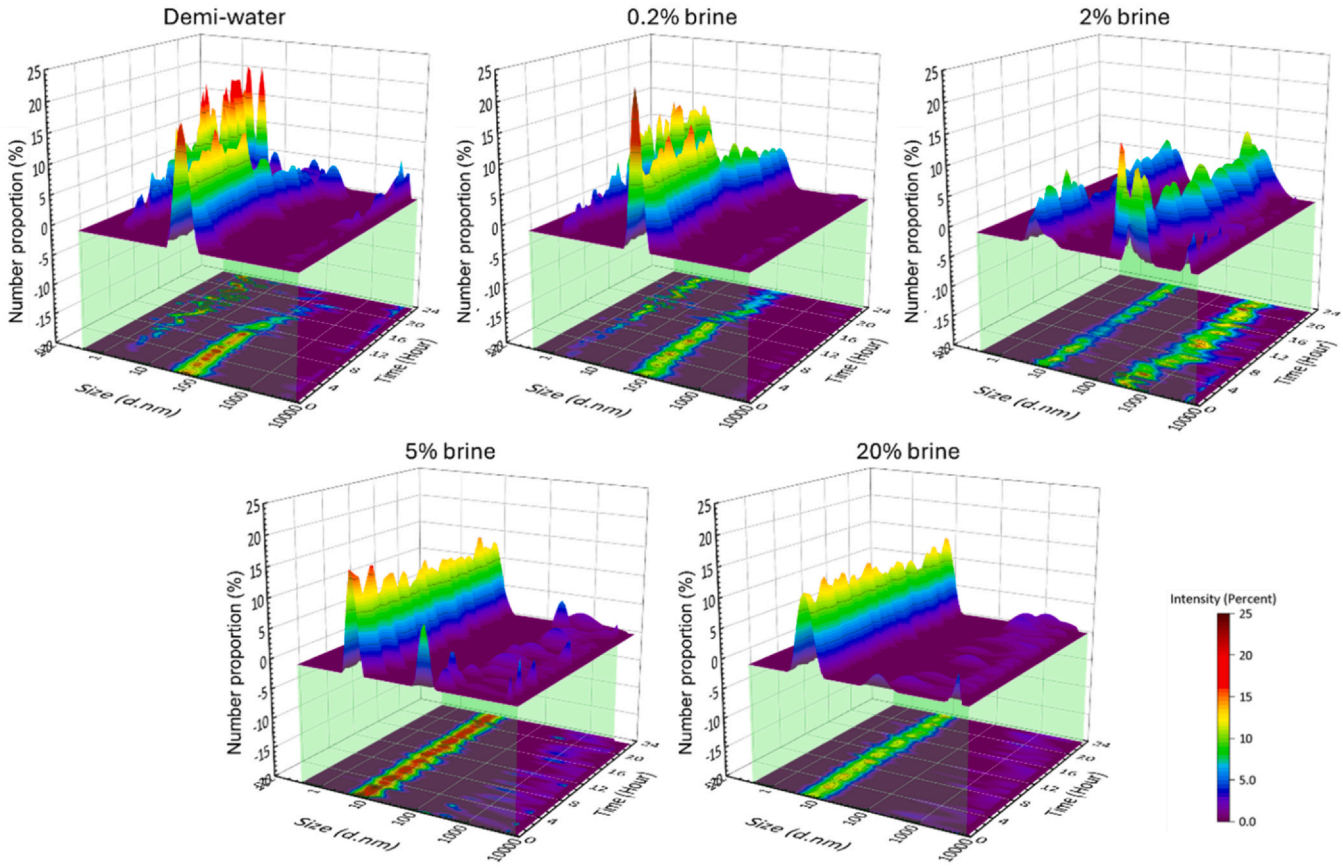

Fig. 10. Dynamic changes in emulsion droplet size over time in a system of dodecane with SPAN 80.

dominant, steadily increasing in both size and number of proportion. During this period, the larger emulsion droplets (blue triangles, 1000–10000 nm) remain present but in much smaller numbers. The system seems to reach a transitional state, with both small and middle-sized droplets coexisting, while the large droplets become less significant. Between 10 and 15 h, the small-size emulsion droplets experience rapid growth, catching up with the middle-size droplets in terms of number of proportion. This increase corresponds to the ongoing formation of small droplets due to continued emulsification at the oil-water interface. The large emulsion droplets, by contrast, show more fluctuations, indicating that their stability is relatively poor compared to the smaller droplets. At 15–24 h, the emulsion system reaches a steady state where the small and middle-size emulsion droplets dominate, each contributing roughly equal proportions. The mean size (yellow dashed line) shows a steady status during this time, reflecting the stabilization of the emulsion sizes.

4.2. Effect of salinity on nano-scale emulsification

To better understand the effect of salinity on emulsion droplet size, the dynamic changes in emulsion droplet size distribution is captured over time for dodecane with SPAN 80 under five different salinity conditions: 0 %, 1.7 %, 17 %, 5 %, and 20 % salinity, as shown in Fig. 10. The 3D plots clearly show how the size and number proportion of emulsion droplets evolve during the emulsification process, which highlights the critical role that salinity plays in the formation and stability of emulsion droplets.

We can see that, certainly at the beginning, the size distribution of medium-size droplets (100–1000 nm) in the case of demi water is wider than the case of 0.2 % salinity At later times (around 12 h), more small-size are formed in the demi water case than 0.2 % salinity case. This explains why the bottle with demi water in Fig. 6 has clearer interface than it in the bottle with 0.2 % brine; it has small micelles. The case of 2 % brine shows more stable emulsion droplets than the lower salt concentration. From beginning to the end, the small-size and middle-size emulsion droplets show similar behaviour, which indicates that this salt concentration provides higher stability for the emulsification. With the increase in salinity, emulsion droplets tend to shrink in size but very stable. 20 % brine only has a narrow range of small-size emulsion droplets (smaller than 10 nm). The behaviour of emulsion droplets observed in this figure correlates with visual observations of emulsion droplets in Fig. 6, where increased salinity generally leads to smaller droplets. This is because higher ionic strength promotes micelle formation and stabilizes smaller droplets, reducing coalescence and maintaining smaller emulsion droplet sizes. However, there is an optimal salinity for the emulsion repelling at the oil-brine interface, as shown in the picture of 0.2 % brine in Fig. 6.

Fig. 11 provides the dynamic changes in emulsion droplet size for the experiments with heptane + SPAN80. In general, the trend and salinity are similar with the above case with dodecane. Comparing the results of DIW between heptane and dodecane, heptane induces a larger mean size of emulsion droplets (442 nm) in the beginning than dodecane (53 nm). The 0.2 % and 2 % brine also have the same phenomenon, which reflects the results of Fig. 6, where the emulsion layers with heptane/low-salt brine are whiter and thicker than those with dodecane. Another worth-noting point in Fig. 11 is that the number proportion of emulsion peaks in every case is higher around 5 % than it in the cases of dodecane experiment. Additionally, the emulsion droplets in 5 % brine shows wider range than it in dodecane. Nevertheless, 5 % and 20 % brine salts induce the stable emulsion droplets comprised of small-size (1–10 nm), which indicates a higher salinity reduces the emulsion swelling and inhibits the emulsion aggregation. This phenomenon is consistent with the proposed mechanisms of salinity effect on emulsion generation at the water-oil interface in the literature

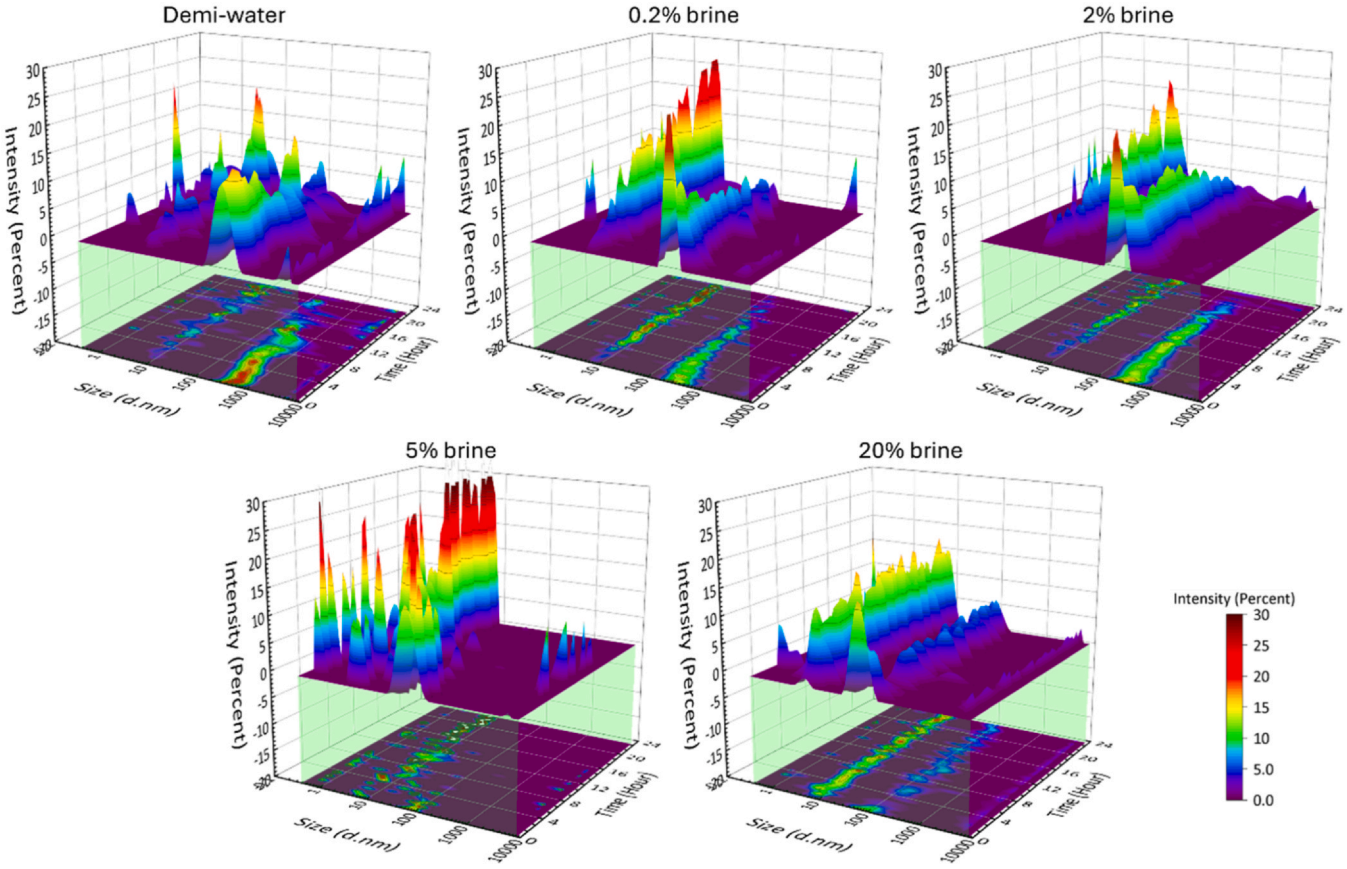

Fig. 11. Dynamic changes in emulsion droplet size over time in a system of heptane with SPAN 80.

(Behera et al., 2014; Davis et al., 2020). Compared to heptane, dodecane has a better performance on the stability of emulsion formation and swelling in salt environments.

4.3. Direct observation of spontaneous emulsification at micro scale

Through the pendant drop experiments, one can gain a detailed observation of the dynamic emulsification process. We have done that over 13 h for a DIW pendant drop in the environment of dodecane + 1 % SPAN 80 surfactant. Fig. 12 highlights the key stages of emulsion formation at the oil-water interface and provides valuable insights into the underlying mechanisms of spontaneous emulsification. At 0 h, the pendant drop is visibly smooth and symmetrical, indicating that no significant emulsification has yet occurred. By 2 h, the surface of the droplet exhibits noticeable non-uniformity. The zoomed-in section reveals a distinct protrusion forming on the droplet's surface, suggesting the initial stages of emulsion formation. This protrusion is a direct result of micelle aggregation at the oil-water interface, driven by the surfactant's activity. As micelles accumulate and interact, they lead to the growth of microemulsion droplets, which begin to distort the droplet's surface. This growth is accompanied by an imbalance between gravitational, surface tension, and buoyancy forces, ultimately leading

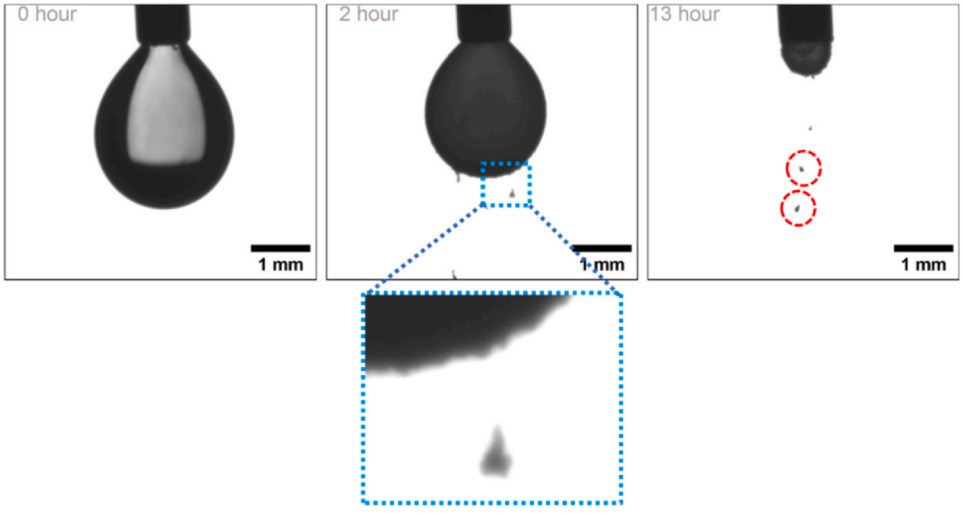

Fig. 12. Key stages of emulsion formation at the oil-water interface during 13 h for a DIW droplet in the solution of dodecane + 1 % SPAN 80 solution.

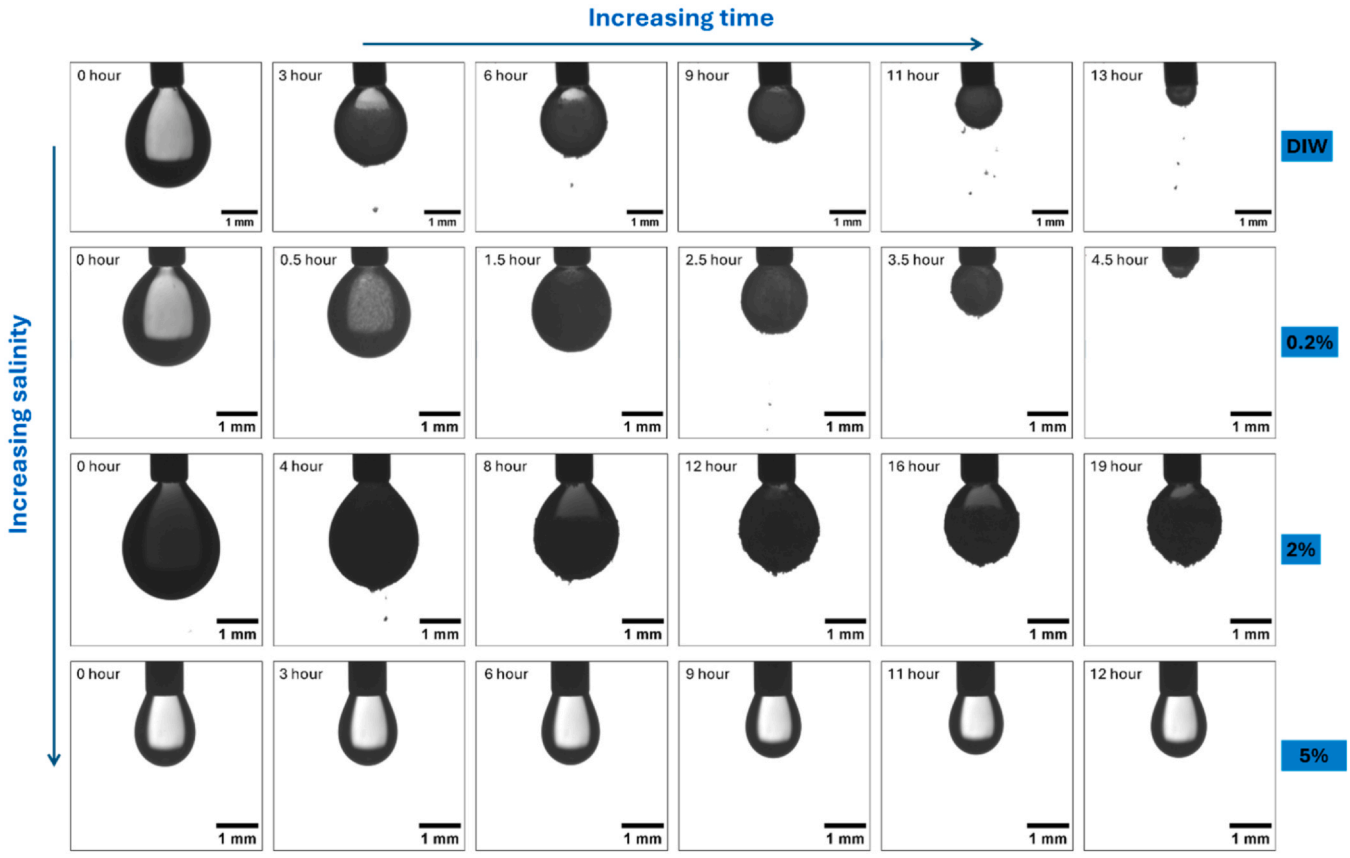

Fig. 13. Visualization of the impact of salinity on the dynamic process of spontaneous emulsification in a system consisting of dodecane and 1 % SPAN 80.

to the detachment of emulsion droplets from the main droplet. These flakes (in the blue-dashed region) are the result of accumulated emulsion droplets breaking away due to the continued imbalance of forces at the interface. The detachment of these emulsion droplets reduce the overall size of the droplet. At 13 h, the process of emulsion formation has progressed significantly. The droplet shrinks into a small size and the surface has become even more irregular, and small emulsion flakes are visibly detaching from the bottom of the droplet, as indicated by the red dashed circles. The presence of these flakes indicates that the system is reaching a state of dynamic equilibrium, where the formation and detachment of emulsion droplets continue at a steady rate.

Fig. 13 provides a comprehensive visualization of the impact of salinity on the dynamic process of spontaneous emulsification in a system consisting of dodecane and 1 % SPAN 80. The figure presents the evolution of a pendant water droplet in environments of increasing brine salinity (from deionized water to 5 % brine), with time progressing from left to right. The observations offer insights into how salinity governs the emulsification behaviour and the resulting changes in droplet morphology over time. In the first row (DIW), the deionized water droplet exhibits significant changes throughout the observation period. Initially, the droplet maintains a smooth shape. However, after 3–6 h, notable emulsification occurs at the interface, marked by the generation of visible emulsion flakes that gradually detach from the droplet. By 13 h, the droplet exhibits pronounced shrinkage, indicative of the active emulsification process, where emulsion droplets formation is more prominent, leading to droplet instability and reduction in size. In the second row (0.2 % brine), emulsification is initiated at a much earlier stage compared to DIW. The first signs of emulsion formation are observable at 0.5 h, and the rate of emulsification progresses rapidly. By 4.5 h, the droplet has already undergone significant shrinkage, suggesting that moderate salinity accelerates the emulsification process. This behaviour implies that low salt concentration enhances micelle activity at the oil-water interface, resulting in faster droplet deformation and emulsification. The third row (2 % brine) exhibits a clear transition in behaviour. The droplet remains relatively stable for a longer period, with only moderate shrinkage observed by 16 h. The emulsion layer is less pronounced compared to lower salinity conditions, reflecting the inhibitory effect of higher salinity on emulsification. The increased ionic strength of the brine likely stabilizes the interface by reducing micelle formation and hindering the diffusion of micelles into the oil phase. The fourth row (5 % brine) displays the most stable behaviour, with the droplet exhibiting minimal changes in size and shape over the entire 12-hour observation period. No visible emulsion formation or detachment of emulsion flakes is observed. This stability suggests that high salinity significantly suppresses spontaneous emulsification. The elevated ionic concentration in the brine likely strengthens electrostatic interactions at the oil-water interface, thereby preventing micelle activity and stabilizing the droplet structure. Overall, the results presented in Fig. 13 clearly demonstrate that lower salinity levels (DIW and 0.2 % brine) promote more active emulsification and droplet shrinkage, whereas higher salinity levels (2 % and 5 % brine) lead to increased interface stability. These findings are consistent with the understanding that salinity impacts the formation and diffusion of micelles, which in turn influences the emulsification process.

Fig. 14 illustrates the influence of salinity on the spontaneous emulsification process in a system consisting of heptane and 1 % SPAN 80. The images capture the morphological changes in a pendant water droplet at the oil-brine interface. In the first row (DIW), the deionized water droplet demonstrates rapid emulsification. At 0 h, the droplet appears smooth and stable, but by 0.5–1 h, emulsification becomes evident as the droplet begins to deform, and emulsified particles detach from the surface. By 4 h, significant droplet shrinkage and detachment of emulsion flakes can be observed. This behaviour closely mirrors that seen in the dodecane system (Fig. 13), where DIW also exhibited

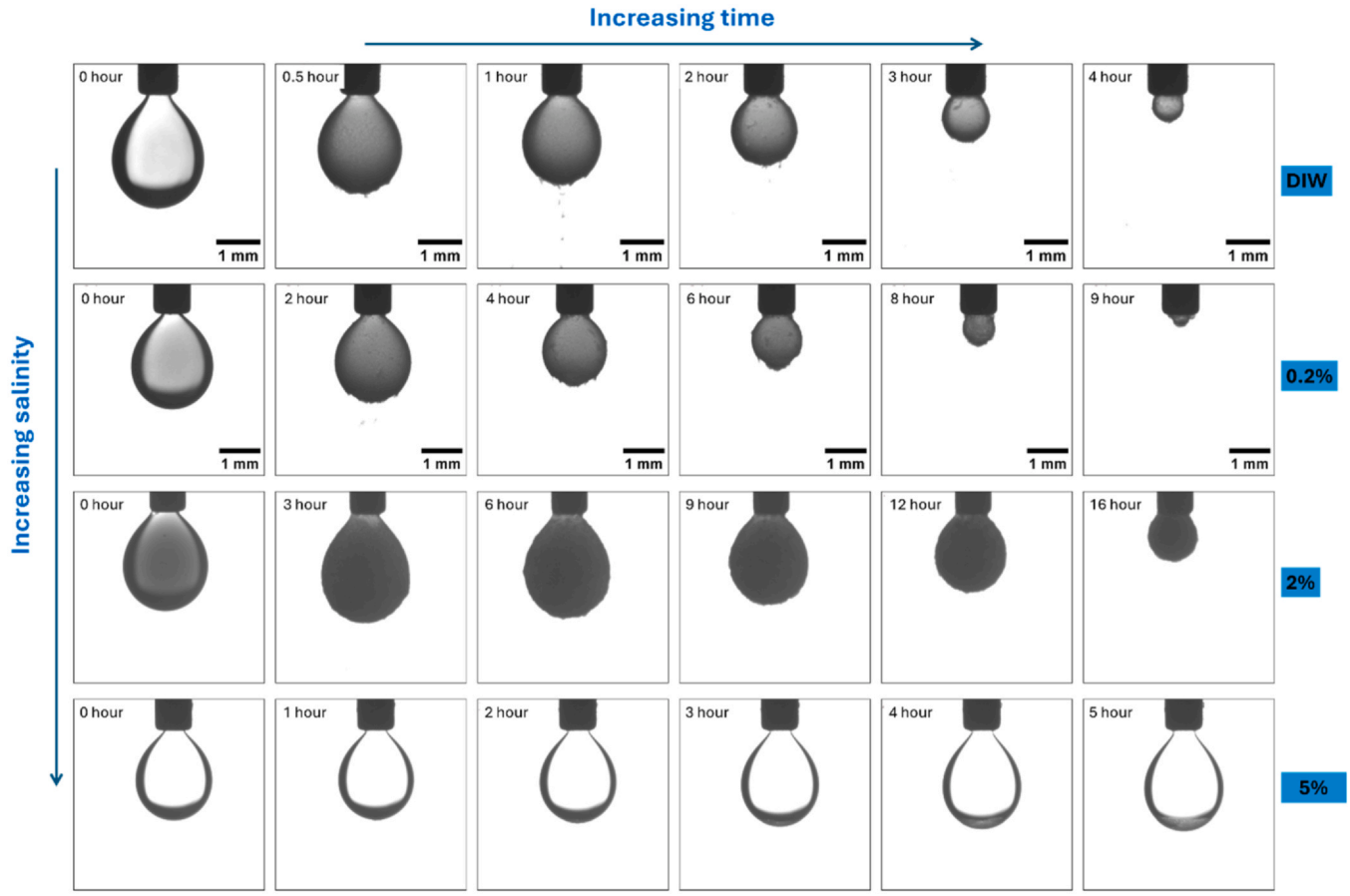

Fig. 14. Visualization of the impact of salinity on the dynamic process of spontaneous emulsification in a system consisting of heptane and 1 % SPAN 80.

accelerated emulsification and substantial droplet reduction. In the second row (0.2 % brine), emulsification proceeds at a slower pace compared to DIW. Emulsion formation becomes visible between 2 and 4 h, and although shrinkage is evident by 8–9 h, the process is notably delayed compared to the DIW case. The presence of 1.7 g/L salinity introduces moderate stabilization to the droplet, reducing the rate of emulsification while still allowing for droplet shrinkage over time. This trend aligns with the observations from dodecane, where low salinity similarly delayed emulsification but did not fully suppress it. In the third row (2 % brine), the droplet exhibits significant stability, with minimal emulsification occurring even after 6–12 h. By 16 h, only a slight reduction in droplet size is observed, and a relatively thick emulsion layer forms around the surface. The higher salinity inhibits micelle formation, suppressing spontaneous emulsification and maintaining droplet integrity for a prolonged period. This stabilization effect is comparable to that seen in dodecane, where the 5 % brine condition similarly hindered emulsification, preserving the droplet structure. In the fourth row (5 % brine), the droplet remains highly stable throughout the entire observation period. Even after 5 h, there is no visible emulsification or droplet deformation, indicating that high salinity effectively prevents the formation of emulsion droplets at the oil-brine interface. This behaviour is consistent with the dodecane system, where high salinity levels similarly suppressed emulsification and preserved droplet stability.

However, the rate of emulsification appears to be slightly faster in the heptane system, with observable changes occurring earlier, especially in the DIW and 0.2 % brine conditions. This suggests that heptane may facilitate faster emulsification at lower salinities compared to dodecane, although both follow the same general pattern of salinity-dependent behaviour. This is also consistent with the observation in the DLS experiments in Section 4.2 Salinity has a profound effect on spontaneous emulsification in both heptane and dodecane systems. Lower salinities promote emulsification and droplet shrinkage, while higher salinities suppress emulsification and stabilize the droplet.

4.4. Effect of salt concentrations in micro-scale emulsification

Fig. 15 provides a detailed analysis of the kinetics of emulsification in dodecane + SPAN 80 and heptane + SPAN 80 systems, using four brine solutions of varying salinity (DIW, 0.2 %, 2 %, and 5 %). The figure includes three subplots: (a) the measured interfacial tension (IFT) over time, (b) the ratio of emulsion volume to initial droplet volume, and (c) the calculated emulsion generation rate. The emulsion volume ($V_{emulsion}$) is considered as the same shrinkage volume of droplet (ΔV_{drop}). Thus, the dimensionless value of the emulsion volume can be calculated as, $V_{emulsion}/V_0$ where V_0 is the initial volume of droplet. This calculation allows us to directly evaluate the impact of salt concentration on the emulsification. Based on the results in the DLS experiment, it is assumed that the average diameters of emulsion for dodecane and heptane are 150 nm and 250 nm, respectively, which helps us to calculate the dynamic numbers of generated emulsion. Given that the droplet is close to a spherical shape with a diameter r, the formation rate of emulsion is considered as, $\frac{\Delta V_{drop}}{\Delta t}\frac{3}{4\pi r^3}$.

In the dodecane + SPAN 80 system, the initial IFT values range from 3.11 mN/m to 4.59 mN/m, indicating that the oil-brine interface is initially similar across all salinity levels. Over time, the IFT decreases sharply for lower salinities (DIW and 0.2 %), reflecting rapid emulsification. Specifically, the IFT for DIW and 0.2 % drops to around 0.14 mN/m within the first 20 h. In contrast, the higher salinity brines (2 % and 5 %) exhibit a much slower decline in IFT, with 5 % maintaining a relatively stable value of around 0.8 mN/m after an initial drop,

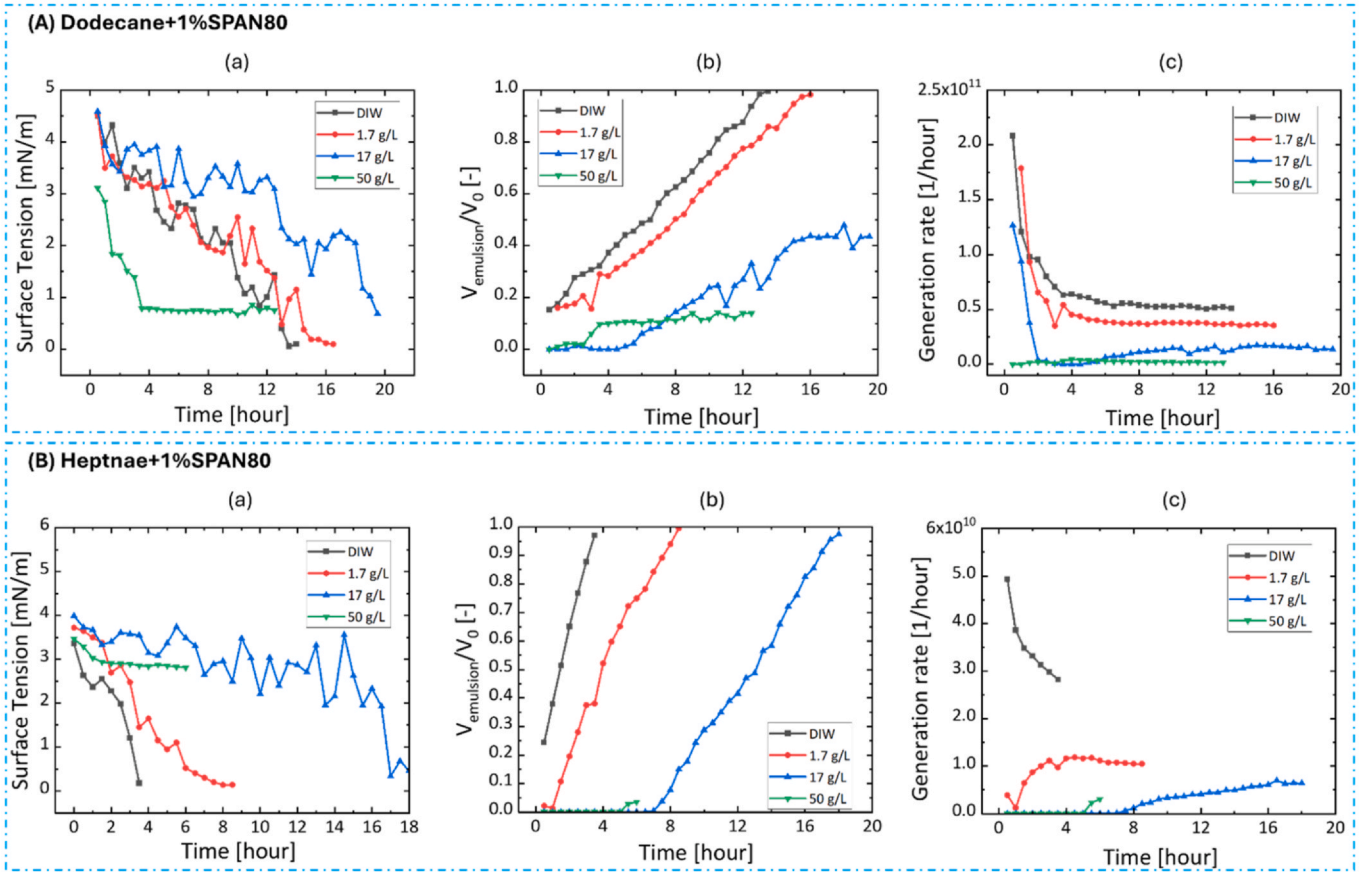

Fig. 15. Kinetics of emulsion droplets in the environments of dodecane + SPAN80 and heptane + SPN80. (a), measured surface tension for four brine droplets; (b), ratio of emulsion volume and initial droplet volume; (c), the calculation for the generation rate of emulsion numbers with four brines.

indicating minimal emulsification. For dodecane, the ratio of emulsion volume to initial droplet volume increases quickly for DIW and 0.2 %, indicating significant emulsion formation. This is consistent with the rapid IFT decline, which facilitates the creation of emulsion droplets. At higher salinities (2 % and 5 %), the IFT decline in dodecane + SPAN 80 is slower, with 5 % stabilizing around 0.8 mN/m after an initial drop. Notably, the 5 % brine shows a faster early IFT decline than 2 %, unlike in the heptane system. This is likely due to dodecane's longer chain and polarity, which promote better surfactant packing and micelle rearrangement under high salinity, causing a quicker initial drop. However, the plateau indicates limited further emulsification, reflecting the inhibitory effect of high salt on sustained droplet formation. In contrast, 5 % brine exhibits very little change in emulsion volume, reflecting its inhibitory effect on emulsification. The 2 % brine shows moderate growth in emulsion volume, demonstrating an intermediate emulsification rate. The emulsion generation rate is highest for DIW and 0.2 % brines in the dodecane system, confirming that lower salinity promotes rapid emulsification. The 5 % brine exhibits almost no increase in emulsion generation, while 2 % shows moderate activity. These results suggest that low salinity leads to faster emulsification, while high salinity significantly hinders the process.

In the heptane + SPAN 80 system, the initial IFT values are similar to those in the dodecane system, around 3.5–4 mN/m. However, the rate of IFT decrease for DIW and 0.2 % is even more pronounced in heptane, with IFT values dropping rapidly in the first few hours. The 5 % brine again shows a relatively stable IFT after an initial decrease, with a final value of around 2.8 mN/m, suggesting limited emulsification. The 2 % brine demonstrates an intermediate decrease in IFT, similar to its behaviour in dodecane. The emulsion volume for DIW and 0.2 % increases rapidly. However, the increase occurs even more quickly than in dodecane, indicating faster emulsification in the heptane system. The 2 % brine again shows moderate emulsification behaviour. The 5 % brine shows minimal emulsion volume change, reflecting its stabilizing effect on the droplet. The emulsion generation rate for DIW and 0.2 % is lower than in the dodecane system, with a rapid spike early in the observation period. This suggests that emulsification occurs faster in heptane, particularly at low salinity levels, but the formed emulsion numbers in one hour (maximum 5×10^{10} in DIW) are lower than in dodecane (maximum 2×10^{11} in DIW). The 5 % brine again shows almost no emulsion generation, while 2 % demonstrates moderate activity, similar to its behaviour in dodecane.

4.5. Proposed theory of salinity effect on spontaneous emulsification

Fig. 16 illustrates four distinct scenarios related to the impact of salinity on water-in-oil emulsification behaviour in the presence of a surfactant. These scenarios reflect how varying salinity levels in the brine phase influence micelle formation, diffusion, and the overall stability of the oil-brine interface.

In the first scenario, where the aqueous phase consists of pure water, spontaneous emulsification in the oil phase containing a surfactant (Span 80) starts as soon as the oil comes into contact with the water. Initially, the reverse micelles are formed in the oil phase as there we have the surfactant in oil phase. Water diffuses across the interface from the water phase into the oil phase. As micelles are formed, they withdraw water free molecules that were dissolved in the oil phase, which prompts the diffusion of water molecules from the water phase. This also explains why we have less emulsification when salinity is higher. Higher salt concentration impedes the migration of water molecules across the interface, as salt ions surround and hold water molecules. Adsorption of surfactants on the oil-water interface reduces interfacial tension and allows water molecules to diffuse easier into the oil phase.

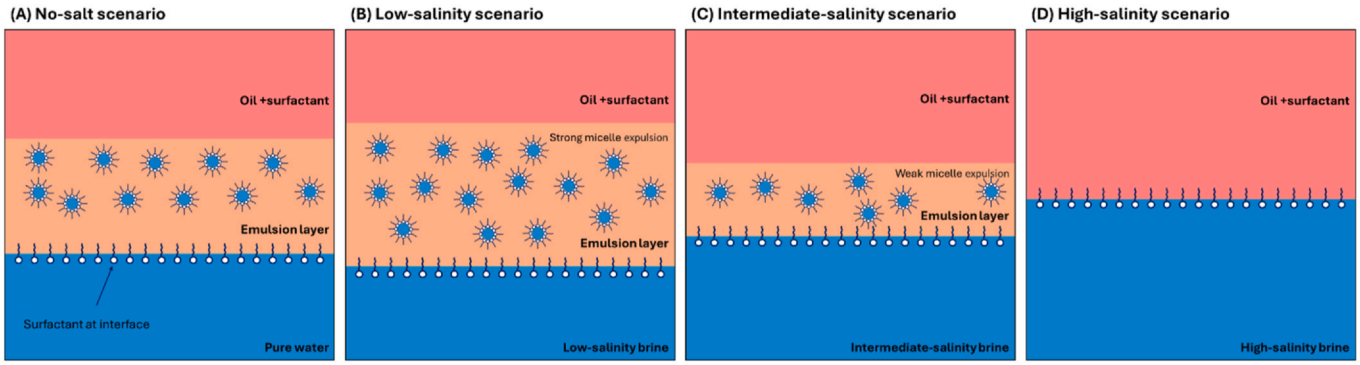

Fig. 16. Four scenarios for the impact of salt on water-in-oil emulsion behaviour.

The spontaneous emulsification process is governed by thermodynamic, as the system naturally moves towards a state of lower free energy. However, due to the lack of ionic interference and electrostatic forces among reverse micelles, a large-extension emulsion layer does not form in the oil phase.

As the salinity of the brine increases further, as shown in the third scenario, the impact of the salt ions becomes much more significant. The higher ionic concentration strengthens electrostatic interactions at the interface, leading to greater hindrance of reverse micelle diffusion. This behaviour is governed by the Debye length (the distance over which electrostatic forces are screened in the presence of ions). As salinity increases, the Debye length shortens, meaning that charged particles (like reverse micelles) experience stronger repulsive forces over shorter distances (Riccardi and Tichelkamp, 2019). The stronger electrostatic interactions between the charged surfactant reverse micelles and the hydrated ions at the interface weaken reverse micelle exclusion into the oil phase (Sofla et al., 2016). As a result, the emulsion layer that forms are thinner, and the rate of spontaneous emulsification is slower. The presence of ions prevent reverse micelles can migrate into the oil. At high salt levels, ions crowd near the interface and compress the electrical double layer, reducing the Debye length. This stronger, localized electrostatic repulsion limits reverse micelle movement and surfactant rearrangement, keeping the interfacial tension high and stable. As a result, the interface becomes more rigid, suppressing emulsification and maintaining minimal micelle activity.

In the fourth scenario, a high-salinity brine is used, with a significantly higher concentration of salt ions in the aqueous phase. This leads to the formation of a highly stable interface where reverse micelle formation and diffusion are effectively inhibited. The high concentration of ions creates strong electrostatic forces that prevent the surfactant molecules from lowering the interfacial tension sufficiently to promote emulsification. In this case, the system achieves a stable interfacial state in which no significant spontaneous emulsification occurs. The electrostatic stabilization leads to a barrier for reverse micelle activity, which reduces the overall rate of emulsification to almost zero.

5. Conclusions

In summary, this paper provides a comprehensive study on the impact of salinity on spontaneous emulsification at the water/oil interface, offering both experimental insights and proposed theory. Through two experimental setups, dynamic light scattering setup and pendant drop setup, direct observations of spontaneous emulsification at nano-scale and micro-scale are captured. Based on the results, the influence of five varying salinity on water-in-oil emulsions are detailly evaluated. In addition, the theory of water transport though reserves reverse micelle is illustrated, which contributes to understand better on the experimental phenomenon.

The DLS experiments demonstrate that emulsification gradually begins after 1 h of contact between dodecane + SPAN 80 and 0.2 % brine. The data indicates that the system favours the formation of small and medium-sized emulsions as it approaches equilibrium, suggesting stable reverse micelle diffusion and emulsion formation at the oil-brine interface. In addition, salinity's impact on emulsification is explored under varying salt concentrations (DIW, 0.2 %, 2 %, and 5 %). Higher salinity reduces emulsion size, stabilizing smaller droplets and promoting reverse micelle formation. At lower salinity levels (e.g., 0.2 % brine), the emulsification process results in significant aggregation and growth of both small and medium-sized droplets. Besides, the heptane with shorter hydrocarbon length induces a relative larger mean size of emulsions comparing to the dodecane. This study addresses that gap by providing a comprehensive examination of how emulsion sizes evolve over time, particularly focusing on the kinetics of reverse micelle formation and diffusion under varying salinity conditions.

In the pendant drop experiments, the dynamic emulsification processes in dodecane and heptane systems with 1 % SPAN 80 are observed. Results suggest that heptane promotes faster emulsification compared to dodecane at lower salinities. The experiments also highlight the critical role of salinity in the emulsification process. In both dodecane and heptane systems, lower salinity levels (DIW and 0.2 % brine) result in rapid emulsification, with significant droplet shrinkage and active reverse micelle-driven emulsification. Higher salinities (2 % and 5 % brine) stabilize the oil-water interface, suppressing emulsification and maintaining droplet size. While the overall pattern is consistent between the two oils, emulsification occurs slightly faster in the heptane system, particularly at lower salinities, although the total number of emulsions formed in heptane is lower compared to dodecane. These results indicate that salinity controls reverse micelle formation and diffusion, and higher salinities significantly hinder emulsification by stabilizing the interface through increased electrostatic interactions.

Given the strong influence of salinity on emulsification dynamics, these findings contribute to better understanding on the mechanism of low-salinity water flooding for enhanced hydrocarbon recovery. By adjusting brine salinity, operators can influence reverse micelle activity and emulsification rates, enhancing oil displacement efficiency. Furthermore, the study suggests that the role of surfactant type and oil-solubility should be explored further to understand their combined effects with salinity.

CRediT authorship contribution statement

Lifei Yan: Writing – review & editing, Writing – original draft, Software, Methodology, Formal analysis, Data curation, Conceptualization. **Amir Raoof:** Supervision, Conceptualization. **Senyou An:** Writing – review & editing, Conceptualization.

Declaration of Competing Interest

The authors declare that they have no known competing financial interests or personal relationships that could have appeared to influence the work reported in this paper.

Acknowledgments

The last author would like to thank the funding from National Natural Science Foundation of China (Grant No. 52474105).

References

Bahtz, J., Gunes, D.Z., Syrbe, A., Mosca, N., Fischer, P., Windhab, E.J., 2016. Quantification of spontaneous W/O emulsification and its impact on the swelling kinetics of multiple W/O/W emulsions. Langmuir 32 (23), 5787–5795.

Behera, M.R., Varade, S.R., Ghosh, P., Paul, P., Negi, A.S., 2014. Foaming in micellar solutions: effects of surfactant, salt, and oil concentrations. Ind. Eng. Chem. Res. 53 (48), 18497–18507.

Cheng, J., Chen, J.-F., Zhao, M., Luo, Q., Wen, L.-X., Papadopoulos, K.D., 2007. Transport of ions through the oil phase of W1/O/W2 double emulsions. J. Colloid Interface Sci. 305 (1), 175–182.

Davis, C.R., Martinez, C.J., Howarter, J.A., Erk, K.A., 2020. Diffusion-controlled spontaneous emulsification of water-soluble oils via micelle swelling. Langmuir 36 (26), 7517–7527.

Du, Y., Xu, K., Mejia, L., Zhu, P., Balhoff, M.T., 2019. Microfluidic investigation of low-salinity effects during oil recovery: a no-clay and time-dependent mechanism. SPE J.

Goyal, P., Aswal, V., 2001. Micellar structure and inter-micelle interactions in micellar solutions: results of small angle neutron scattering studies. Curr. Sci. 80 (8), 972–979.

Israelachvili, J.N., 2011. Intermolecular and Surface Forces. Academic Press.

Kokal, S., 2005. Crude-oil emulsions: a state-of-the-art review. SPE Prod. Facil. 20 (01), 5–13.

Li, Z., Xu, D., Yuan, Y., Wu, H., Hou, J., Kang, W., Bai, B., 2020. Advances of spontaneous emulsification and its important applications in enhanced oil recovery process. Adv. Colloid Interface Sci. 277, 102119.

López-Montilla, J.C., Herrera-Morales, P.E., Pandey, S., Shah, D.O., 2002. Spontaneous emulsification: mechanisms, physicochemical aspects, modeling, and applications. J. Dispers. Sci. Technol. 23 (1-3), 219–268.

Maaref, S., Ayatollahi, S., 2018. The effect of brine salinity on water-in-oil emulsion stability through droplet size distribution analysis: a case study. J. Dispers. Sci. Technol. 39 (5), 721–733.

Martínez-Palou, R., Cerón-Camacho, R., Chávez, B., Vallejo, A.A., Villanueva-Negrete, D., Castellanos, J., Karamath, J., Reyes, J., Aburto, J., 2013. Demulsification of heavy crude oil-in-water emulsions: a comparative study between microwave and thermal heating. Fuel 113, 407–414.

Pays, K., Giermanska-Kahn, J., Pouligny, B., Bibette, J., Leal-Calderon, F., 2002. Double emulsions: how does release occur? J. Control. Release 79 (1-3), 193–205.

Peltonen, L., Hirvonen, J., Yliruusi, J., 2001. The behavior of sorbitan surfactants at the water–oil interface: straight-chained hydrocarbons from pentane to dodecane as an oil phase. J. Colloid Interface Sci. 240 (1), 272–276.

Riccardi, E., Tichelkamp, T., 2019. Calcium ion effects on the water/oil interface in the presence of anionic surfactants. Colloids Surf. A Physicochem. Eng. Asp. 573, 246–254.

Rodríguez-Hakim, M., Anand, S., Tajuelo, J., Yao, Z., Kannan, A., Fuller, G.G., 2020. Asphaltene-induced spontaneous emulsification: Effects of interfacial co-adsorption and viscoelasticity. J. Rheol. 64 (4), 799–816.

Rosen, M.J., Kunjappu, J.T., 2012. Surfactants and Interfacial Phenomena. John Wiley & Sons.

Salehpour, M., Sakhaei, Z., Salehinezhad, R., Mahani, H., Riazi, M., 2021. Contribution of water-in-oil emulsion formation and pressure fluctuations to low salinity water-flooding of asphaltic oils: a pore-scale perspective. J. Pet. Sci. Eng. 203, 108597.

Sofla, S.J.D., Sharifi, M., Sarapardeh, A.H., 2016. Toward mechanistic understanding of natural surfactant flooding in enhanced oil recovery processes: the role of salinity, surfactant concentration and rock type. J. Mol. Liq. 222, 632–639.

Stone, H.A., 1994. Dynamics of drop deformation and breakup in viscous fluids. Annu. Rev. Fluid Mech. 26 (1), 65–102.

Wen, L., Papadopoulos, K.D., 2000. Visualization of water transport in W1/O/W2 emulsions. Colloids Surf. A Physicochem. Eng. Asp. 174 (1-2), 159–167.

Yan, L., Aslannejad, H., Hassanizadeh, S.M., Raoof, A., 2020. Impact of water salinity differential on a crude oil droplet constrained in a capillary: pore-scale mechanisms. Fuel 274, 117798.

Yan, L., Chang, Y., Hassanizadeh, S.M., Xiao, S., Raoof, A., Berg, C.F., He, J., 2022. A quantitative study of salinity effect on water diffusion in n-alkane phases: from pore-scale experiments to molecular dynamic simulation. Fuel 324, 124716.

Yan, L., Golestan, M.H., Zhou, W., Hassanizadeh, S.M., Berg, C.F., Raoof, A., 2023. Direct evidence of salinity difference effect on water transport in oil: pore–scale mechanisms. Energy Fuels 37 (20), 15537–15552.

Zabar, M.K., Nguyen, C.V., Phan, C.M., 2020. Quantifying the influence of salinity on spontaneous emulsification of hydrocarbons. Colloids Surf. A Physicochem. Eng. Asp. 588, 124376.

Zheng, Y., Davis, C.R., Howarter, J.A., Erk, K.A., Martinez, C.J., 2022. Spontaneous emulsions: adjusting spontaneity and phase behavior by hydrophilic–lipophilic difference-guided surfactant, salt, and oil selection. Langmuir 38 (14), 4276–4286.